Optical absorption enhancement in slanted silicon nanocone hole arrays for solar photovoltaics*

Shu-Yuan Zhang(张淑媛), Wen Liu(刘雯), Zhao-Feng Li(李兆峰), Min Liu(刘敏), Yu-Sheng Liu(刘雨生), Xiao-Dong Wang(王晓东)†, and Fu-Hua Yang(杨富华)

Engineering Research Center for Semiconductor Integrated Technology, Institute of Semiconductors, Chinese Academy of Sciences, Beijing 100083, *China*

(Received 11 May 2016; revised manuscript received 17 June 2016; published online 25 August 2016)

We investigate slanted silicon nanocone hole arrays as light absorbing structures for solar photovoltaics via simulation. With only 1-μm equivalent thickness, a maximum short-circuit current density of 34.9 mA/cm^2 is obtained. Moreover, by adding an Ag mirror under the whole structure, a short-circuit current density of 37.9 mA/cm^2 is attained. It is understood that the optical absorption enhancement mainly results from three aspects. First, the silicon nanocone holes provide a highly efficient antireflection effect. Second, after breaking the geometric symmetry, the slanted silicon nanocone hole supports more resonant absorption modes than vertical structures. Third, the Fabry–Perot resonance enhances the light absorption after adding an Ag mirror.

Keywords: photovoltaic, light-trapping structure, simulation

PACS: 68.55.jm, 88.30.gg, 88.40.H– **DOI:** 10.1088/1674-1056/25/10/106802

1. Introduction

Photovoltaic technology is a direct way to capture and harvest solar energy in real-time. As the second-generation photovoltaic cells,[1] thin-film solar cells have become a promising alternative due to its less material consumption and lower manufacturing cost.[2] However, the active layer is too thin to absorb sufficient light without effective light trapping schemes,[3] which results in low solar power conversion efficiency. Therefore, developing light-trapping technologies becomes an effective way to achieve high optical absorption of thin-film solar cells. So far, more and more combinations of different light trapping and antireflection structures have been reported, such as nanoholes (NHs),[4–7] nanowires (NWs),[8–12] nanoparticles (NPs),[13–19] nanocones (NCs),[8,20–23] and nanocone holes(NCHs).[24–30] Recently, Zhang *et al.* attained a short-circuit current density of 31.9 mA/cm^2 with an equivalent thickness of 1-μm silicon by an optimized double-sided vertical NCH structure.[30] However, most of the researches have focused on different combinations of vertical NCHs, only few considered slanted NCHs. As far as we know, only Eyderman *et al.* obtained an impressive short-circuit current density of 35.5 mA/cm^2 within 1 μm equivalent thickness crystalline silicon over the spectral range of 300 nm–1100 nm by investigating slanted conical-pore photonic crystals with an Ag back-reflector.[31] However, the optimum values of taper angles and tilt angles of the slanted conical-pore were not studied in detail, and the influence of the distance between Ag back-reflector and the active layer was not fully investigated.

In this paper, a slanted silicon NCH array is proposed, which is not exactly the same structure as that demonstrated by Eyderman *et al.*[31] A short-circuit current density of 37.9 mA/cm^2 is attained after optimizing the taper angle and tilt angle and adding an Ag mirror under the whole structure. Moreover, the fabrication of the NCH array has received considerable attention currently. But it is hard to achieve a strictly vertical one just as expected. For instance, Zhang *et al.* fabricated highly-ordered silicon NCH arrays by integrating the nanosphere lithography with the reactive ion etching (RIE) method,[28] which turned into a slanted silicon NCH array with different taper angles. Therefore, it is also of practical importance to study the characteristics of slanted silicon NCH array.

2. Simulation details

Figure 1(a) shows the schematic diagrams of the proposed nanostructures. For further enhancing the optical absorption, we locate an Ag back-reflector under the whole silicon NCH array. The total material in the proposed slanted NCH array textured thin film is equal to 1 μm-thick flat thin-film silicon. In our simulation, we first rotate the vertical NCH around the x axis at angle ϕ (the tilt angle of the NCH). Then we adjust the position of NCH to make sure that it is arranged in the silicon unit cell, which is positioned just as shown in Fig. 1(c). After removing the excrescent part above the silicon top surface we obtain the slanted silicon NCH as illustrated in Fig. 1(d). Besides, θ is the taper angle of the NCH and takes different

*Project supported by the National Natural Science Foundation of China (Grant Nos. 61274066, 61474115, and 61504138) and the National High Technology Research and Development Program of China (Grant No. 2014AA032602).

†Corresponding author. E-mail: xdwang@semi.ac.cn

© 2016 Chinese Physical Society and IOP Publishing Ltd

values. For each value, the tilt angle ϕ ranges from 0 to $\theta/2$. Owing to the fact that if $\phi > \theta/2$, the slanted NCH will extend beyond the edge of the silicon unit cell. However, either θ or ϕ is varying, the area of the hole on the silicon top surface (S_{ellipse}) changes. To make sure that we just have one variable at one time, we introduce the filling factor (FF) which is given by $FF = S_{\text{ellipse}}/S_{\text{cell}}$ as illustrated in Fig. 1(b). Here the S_{cell} is the area of silicon unit cell surface, and we keep the FF at $\pi/4$ in this study. Moreover, to set up our structure parameters more intuitively and conveniently in the simulation, we introduce the parameters a, b and h as shown in Figs. 1(b)–1(d). Parameters a and b are the lattice constants of the slanted NCH along the x and y directions, respectively. While h is the height of the silicon unit cell. They are calculated using the following equations (d is the equivalent thickness of silicon):

$$h = \frac{d}{1-\pi/12}, \tag{1}$$

$$a = h\left[\tan\left(\frac{\theta}{2}+\phi\right)+\tan\left(\frac{\theta}{2}-\phi\right)\right], \tag{2}$$

$$b = \frac{2h}{\cos(\theta/2+\phi)}\sin\frac{\theta}{2}. \tag{3}$$

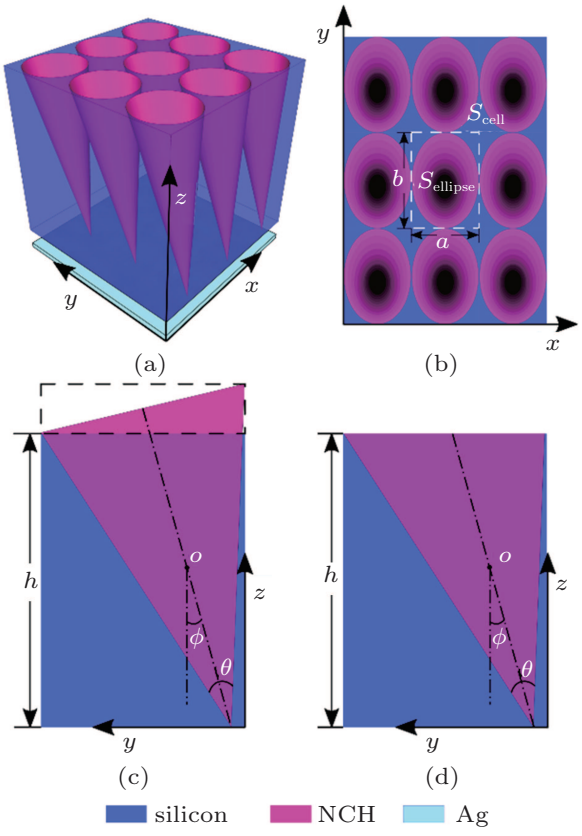


Fig. 1. (color online) (a) Schematic diagram of the proposed slanted NCH array textured silicon thin film layer with an Ag back-reflector located under the bottom of it. (b) The top view of the slanted silicon NCH array. S_{ellipse} represents the area of ellipse, while S_{cell} represents the area of silicon unit cell surface. The filling factor $FF = S_{\text{ellipse}}/S_{\text{cell}}$. a and b are the lattice constants of the slanted NCH along the x and y directions, respectively. Panels (c) and (d) show the side views of the slanted silicon NCH before and after removing the excrescent part. θ and ϕ are the taper angle and tilt angle of the NCH, respectively. The black dashed line is the height of the NCH while O is the middle point of the height. h is the height of the silicon unit cell.

In our work, the electromagnetic field features are numerically analyzed by the finite-difference time-domain (FDTD) method (https://www.lumerical.com/). The dielectric functions are modeled by using a Drude model for Ag and a Drude–Lorentz model for Si. The mesh accuracy is 2. The bottom surface of the textured silicon thin-film is in the x–y plane. The plane wave source is illuminated from the top along the z direction. Periodic boundary conditions are applied to the x and y directions, and perfectly matched layer (PML) boundary conditions are adopted in the z direction. The frequency domain power monitors are placed above and below the thin-film to calculate the reflectance (R) and transmittance (T), respectively. The absorptance (A) is dependent on $A = 1 - R - T$.

3. Simulation results and discussion

In order to obtain the optimum values of taper angles and tilt angles, we first investigate the variation in resonant mode of the silicon NCH array. Figure 2(a) shows the absorption spectra of vertical (the tilt angle $\phi = 0^\circ$) NCH array for different taper angles. It is seen that for each θ, the absorption spectrum presents some spikes especially for the wavelength range of 700 nm–1100 nm. With the increase of θ, the number of spikes first increases and then decreases. Besides, the intensities of spikes are also different from each other. Each spike corresponds to a resonant absorption mode and all these modes help to enhance the absorption. By contrasting the absorption spectra with each other, the absorption spectrum of $\theta = 20^\circ$ presents fewer spikes with higher intensity. The intensities of spikes are lower for the absorption spectra of $\theta = 40^\circ$, $\theta = 50^\circ$, $\theta = 60^\circ$, and $\theta = 70^\circ$. Only the absorption spectrum of $\theta = 30^\circ$ has advantages in both the number and the intensity of spikes, namely, it is possible to achieve a better absorption around $\theta = 30^\circ$. To further analyze the number of resonant modes and its intensity, we take the $\theta = 20^\circ$ NCH array for example to discuss the influence of the tilt angle on resonant mode. As plotted in Fig. 2(b), some spikes turn stronger whereas some become weaker with the increase of ϕ, and moreover, some other spikes each split into two individual ones. As can be seen, from $\phi = 0^\circ$ to $\phi = 2^\circ$, the number of spikes increases while their intensities all decrease. From $\phi = 2^\circ$ to $\phi = 6^\circ$, both the number of spikes and their intensities increase. In addition, from $\phi = 6^\circ$ to $\phi = 10^\circ$, there is no obvious variation in the number of spikes though the intensity of some spikes are different. As is well known, the strict structural symmetry can lead to the degeneration of some resonant modes.[6] The structural symmetry decreases as ϕ increases, while the number of spikes increases within a certain range of ϕ. Therefore, within an appropriate ϕ range, the slanted NCHs provide more resonant modes than the vertical NCHs.

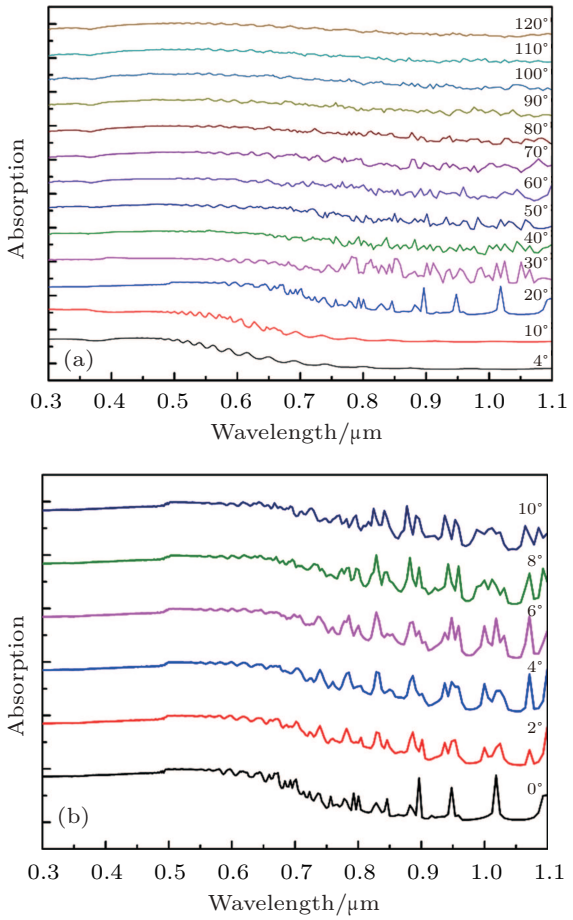


Fig. 2. (color online) (a) Absorption spectra of vertical ($\phi = 0°$) NCH array for different values of taper angle (θ). (b) Absorption spectra of the $\theta = 20°$ NCH array with different values of tilt angle (ϕ). The absorption spectra in panels (a) and (b) are shifted from each other in the vertical axis for clarity.

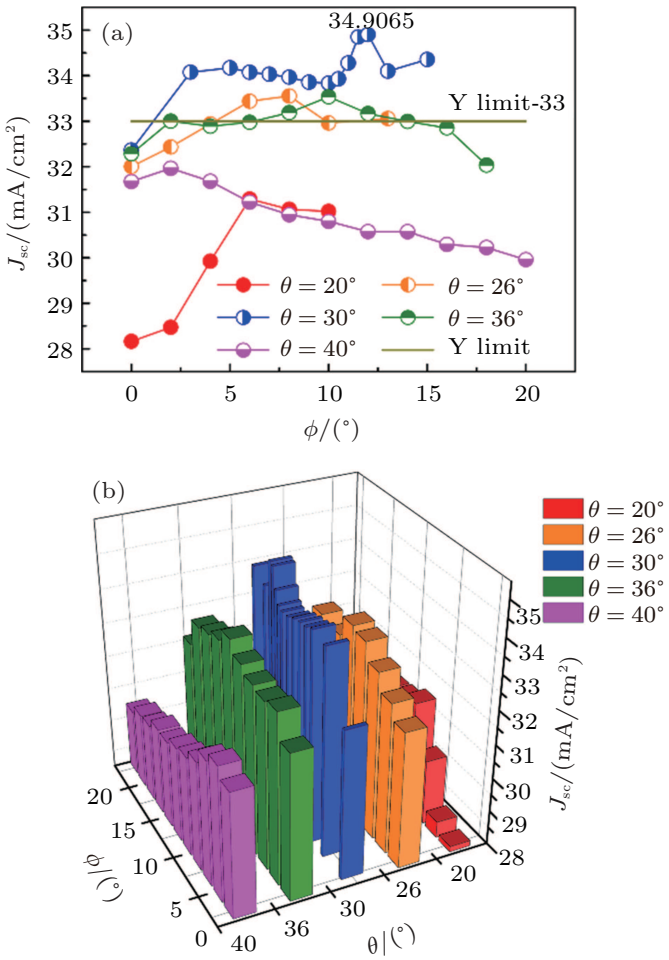


Fig. 3. (color online) (a) Comparison between the short-circuit currents generated by silicon NCHs with different θ and ϕ and the Yablonovitch limit (Y limit). (b) The 3D-histogram of the short-circuit currents under different ϕ values of silicon NCH with different θ values, which is used for visual clarity and sharp contrast.

As is shown in Fig. 2(a), the absorption spectrum of $\theta = 30°$ NCH array shows superiority in both the number and the intensity of resonant modes. It is possible to obtain the optimum values of taper angles and tilt angles around the parameter $\theta = 30°$. Therefore, we take five values for the taper angle θ which are 20°, 26°, 30°, 36° and 40°, respectively. For each value, the NCH will be rotated $0 \sim \theta/2$ degrees and short circuit current density (J_{sc}) will be calculated for each case. As shown in Fig. 3(a), we obtain our best J_{sc} 34.9 mA/cm^2 when $\theta = 30°$ and $\phi = 12°$. Besides, when θ is a constant, the J_{sc} mainly first increases and then decreases as ϕ increases. However, when ϕ is a constant, the J_{sc} first increases with θ and then decreases after the θ has reached a certain value, which is more evident visually in Fig. 3(b). Moreover, in a large range of ϕ, the J_{sc} of the slanted NCH array is larger than that of the vertical ones. In other words, light absorption enhancement of slanted silicon NCH is better than that of the vertical one. Furthermore, for $\theta = 26°$, $\theta = 30°$, and $\theta = 36°$, their J_{sc} values exceed the Yablonovitch limits (Y limit) in a certain range of ϕ. It illustrates that we can gain a high J_{sc} over a large range of θ and ϕ. This also means that the NCH fabrication error is allowed and the manufacturing difficulties are reduced.

For further comparison, we take several solar cells with different light absorbing structures, including a nonpatterned solar cell which serves as a reference, a solar cell with a vertical silicon NCH array ($\theta = 30°$, $\phi = 0°$), and a solar cell with a slanted silicon NCH array ($\theta = 30°$, $\phi = 12°$), labeled as "nonpatterned", "vertical", and "slanted", respectively. To assess the absorption performances of these light absorbing structures, the spectrum of the Yablonovitch limit, namely the theoretical limit of silicon absorption, is also used as another reference. Figure 4 illustrates the absorption enhancements of different configurations. It is seen that the absorptances of the "vertical" and "slanted" cells are significantly enhanced compared with a "nonpatterned" cell over the whole wavelength range investigated. This is mostly attributed to two reasons. Firstly, the gradient of effective index of the NCH array causes the incident light to be reflected at different depths from the interface between air and silicon. As a result, the reflectance is suppressed by destructive interferences. Secondly, the NCH array provides more resonant modes than the nonpatterned silicon thin film. Moreover, the absorptance of the

"slanted" cell is better than that of the "vertical" cell at the long wavelengths, due to the fact that the symmetry breaking of the slanted NCH array induces additional resonant modes and enhances the absorption.[6]

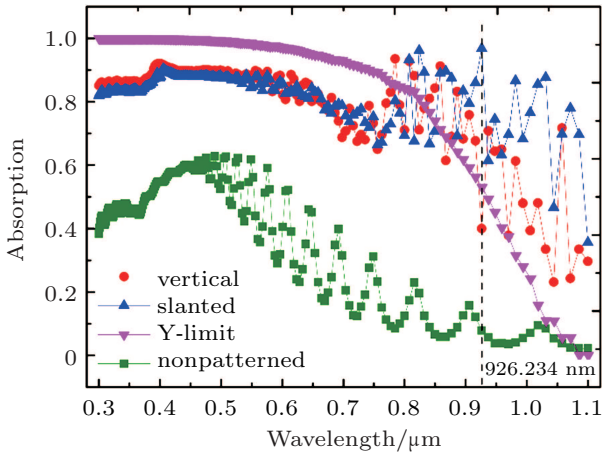


Fig. 4. (color online) Absorption spectra under normal incidence from AM1.5 solar irradiance. The olive square curve represents the absorption spectrum of the nonpatterned solar cell, the pink triangle curve denotes the Yablonovitch limit (labeled as the Y-limit), while the red circle curve and the blue triangle curve refer to the absorption spectra for the "vertical" cell and the "slanted" cell, respectively.

To intuitively understand the physics behind the ultimate device for optical absorption enhancement, the electric-field intensity profiles are analyzed in detail. As shown in Fig. 4, the clear difference of absorptance between the "vertical" and the "slanted" cells appears at the long wavelengths. We take 926.234 nm as a special wavelength of the long wavelengths to study the electric-field intensity, owing to the fact that the difference of absorptance between various cells is biggest at 926.234 nm. For the "nonpatterned" cell of Fig. 5(a), the profile is of typical Fabry–Perot resonance. As shown in Figs. 5(b) and 5(c), a large part of the light is concentrated in the "vertical" and "slanted" cells. This confirms that the absorptances of the "vertical" and "slanted" cells are higher than that of the "nonpatterned" cell. The absorption enhancement results from the antireflection and the optical coupling of the NCHs. In addition, figure 5(c) shows a more extensive and stronger optical absorption concentrating in the silicon around the slanted NCH than around the "vertical" cell. This is attributed to the absorption enhancement of the "slanted" cell in a long wavelength range, which is contributed by the symmetry breaking of the slanted NCH array.

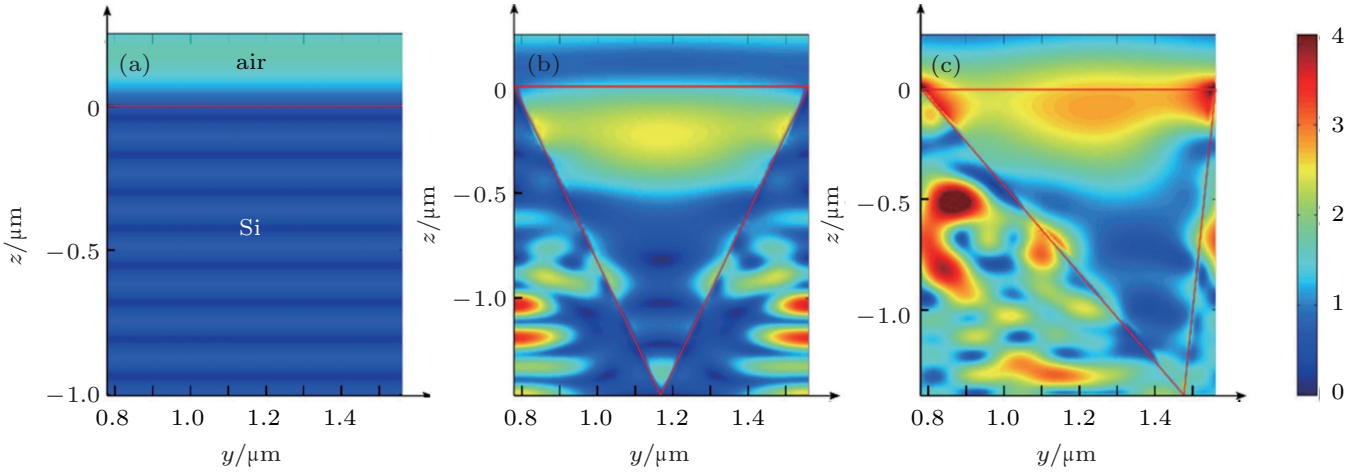


Fig. 5. (color online) Electric-field intensity profiles at 926.234 nm for (a) "nonpatterned" solar cell, (b) "vertical" solar cell, and (c) "slanted" solar cell.

Finally, in order to further improve the short-circuit current density, we add a 100-nm-thick Ag back-reflector under the slanted silicon NCH array, which is labeled as "hybrid" (See Fig. 1(a)). By changing the distance (D) between the active layer and the Ag back-reflector from 0 nm to 3000 nm in steps of 50 nm, a short-circuit current density, 37.9 mA/cm^2, is obtained when $D = 600$ nm as shown in Fig. 6(a). It is seen that the short-circuit current density fluctuates as distance D increases. This is attributed to the Fabry-Perot resonances of light at long wavelengths. It may seem unreasonable that the NCH absorbing structure separates from the Ag back-reflector by an air gap. However, many groups have investigated the detached back-reflector.[32,33] Etienne *et al.* studied the effect of the rear-dielectric/Ag back-reflector design on the optical performance of the thin-film silicon solar cells by means of detached reflectors.[33] One of Etienne *et al.*'s designs is a textured Ag reflector separated from the silicon layer with an air gap.

The absorption spectra of the "hybrid" cell with $D =$ 600 nm and "slanted" cell are shown in Fig. 6(b). It reveals that the absorption enhancement exists in the wavelength range of 500 nm–1100 nm. This is due to the fact that Ag possesses lower absorption loss and the Ag back-reflector can reflect the transmitted light back into the active layer effectively. Moreover, the incident light and the light reflected by the back-reflector can interfere constructively in the active layer, which also contributes to the absorption enhancement.

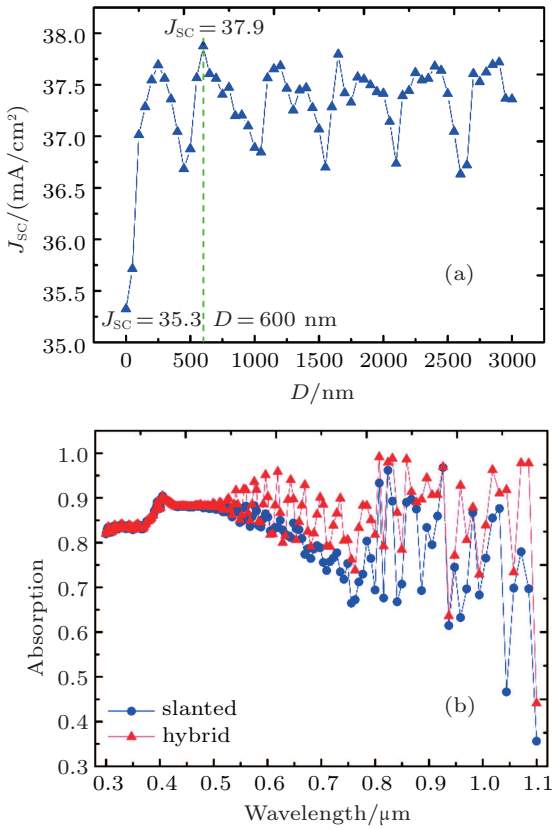


Fig. 6. (color online) (a) Short-circuit current density of the "hybrid" cell as a function of distances D between the active layer and Ag back-reflector. (b) Absorption spectra under normal incidence from AM1.5 solar irradiance. The pink triangle curves and the blue circle curves represent the absorption spectra for the "slanted" cell and the "hybrid" cell, respectively.

4. Conclusions

In this work, the slanted silicon NCH arrays as a light absorbing structure for solar photovoltaics is investigated. The effectiveness of light trapping of the slanted NCH array is presented. First of all, we analyze the variations in resonant modes of the NCH array with different taper angles and tilt angles. Furthermore, we discuss the advantages of the slanted NCHs in light-trapping by comparing with the vertical ones. With our proposed light trapping structure, a thin-film silicon solar cell with a thickness of 1 μm could generate a short-circuit current density of as high as 34.9 mA/cm^2 over the spectral range of 300 nm–1100 nm.

This is attributed to two reasons. Firstly, the gradual changing of the refractive index of the slanted NCH contributes to optical coupling and anti-reflection effects. Secondly, symmetry breaking of the slanted NCH contributes to the generation of resonant modes.[6] Finally, in order to obtain a higher short-circuit current density, we add an Ag back-reflector under the bottom of the NCH structure and discuss the influence of the distance between the Ag mirror and the NCH structure on optical absorption. In an optimal scheme, a short-circuit current density of 37.9 mA/cm^2 is attained. The results of our investigation of the optical properties of the slanted silicon NCH arrays indicate that the slanted NCH array is an efficient light absorbing structure for solar photovoltaics. Our work provides an in-depth understanding of the mechanism of optical absorption enhancement of the slanted silicon NCHs, which may be used in future advanced solar photovoltaics.

References

[1] Green M A 2004 *Solar Energy* **76** 3
[2] Shi Y P, Wang X D, Liu W, Yang T S, Ma J and Yang F H 2014 *Appl. Phys. Express* **7** 062301
[3] Shi Y P, Wang X D, Liu W, Yang T S and Yang F H 2014 *J. Opt.* **16** 075706
[4] Han S E and Chen G 2010 *Nano. Lett.* **10** 1012
[5] Chen Y K, Han W H and Yang F H 2013 *Opt. Lett.* **38** 3973
[6] Lin C, Martinez L J and Povinelli M L 2013 *Opt. Express* **21** *Suppl* **5** A872
[7] Hong L, Rusli, Wang X C, Zheng H Y, Wang H and Yu H Y 2014 *J. Appl. Phys.* **116** 194302
[8] Zhu J, Yu Z F, Burkhard G F, Hsu C M, Connor S T, Xu Y Q, Wang Q, McGehee M, Fan S H and Cui Y 2009 *Nano. Lett.* **9** 279
[9] Garnett E and Yang P D 2010 *Nano. Lett.* **10** 1082
[10] Garnett E C, Brongersma M L, Cui Y and McGehee M D 2011 *Ann. Rev. Mater. Res.* **41** 269
[11] Yue H H, Jia R, Chen C, Ding W C, Wu D Q and Liu X Y 2011 *J. Semicond.* **32** 8
[12] Qiu K, Zuo Y H, Zhou T W, Liu Z, Zheng J, Li C B and Cheng B W 2015 *J. Semicond.* **36** 10
[13] Atwater H A and Polman A 2010 *Nat. Mater.* **9** 205
[14] Beck F J, Mokkapati S, Polman A and Catchpole K R 2010 *Appl. Phys. Lett.* **96** 033113
[15] Liu W, Wang X D, Li Y Q, Geng Z X, Yang F H and Li J M 2011 *Sol. Energy. Mater. Sol. Cells* **95** 693
[16] Xu R, Wang X D, Liu W, Song L, Xu X N, Ji A, Yang F H and Li J M 2012 *Jpn. J. Appl. Phys.* **51** 042301
[17] Shi Y P, Wang X D, Liu W, Yang T S, Xu R and Yang F H 2013 *J. Appl. Phys.* **113** 176101
[18] Chen F X, Wang L S and Xu W Y 2013 *Chin. Phys. B* **22** 045202
[19] Chen L, Wang Q K, Shen X Q, Chen W, Huang K and Liu D M 2015 *Chin. Phys. B* **24** 104201
[20] Jeong S, Garnett E C, Wang S, Yu Z F, Fan S H, Brongersma M L, McGehee M D and Cui Y 2012 *Nano. Lett.* **12** 2971
[21] Wang B M and Leu P W 2012 *Nanotechnology* **23** 194003
[22] Wang K X Z, Yu Z F, Liu V, Cui Y and Fan S H 2012 *Nano. Lett.* **12** 1616
[23] Wang Z Y, Zhang R J, Wang S Y, Lu M, Chen X, Zheng Y X, Chen L Y, Ye Z, Wang C Z and Ho K M 2015 *Sci. Rep.* **5** 7810
[24] Du Q G, Kam C H, Demir H V, Yu H Y and Sun X W 2011 *Opt. Lett.* **36** 1713
[25] Wang W, Zhang J S, Zhang Y, Xie Z and Qin G G 2013 *J. Phys. D: Appl. Phys.* **46** 195106
[26] Xie Z, Wang W, Qin L X, Xu W J and Qin G G 2013 *Opt. Express* **21** 18043
[27] Lin Q F, Leung S F, Lu L F, Chen X Y, Chen Z, Tang H N, Su W J, Li D D and Fan Z Y 2014 *ACS Nano* **8** 6484
[28] Zhang D, Ren W N, Zhu Z C, Zhang H F, Liu B, Shi W Z, Qin X M and Cheng C W 2015 *Nanoscale Res. Lett.* **10** 9
[29] Zhang X, Yu Y G, Xi J T, Liu T L and Sun X H 2015 *J. Opt.* **17** 015901
[30] Zhang X, Yu Y G, Xi J T, Wang Y L and Sun X H 2015 *J. Opt.* **17** 075901
[31] Eyderman S, John S and Deinega A 2013 *J. Appl. Phys.* **113** 154315
[32] Moulin E, Paetzold U W, Siekmann H, Worbs J, Bauer A and Carius R 2011 *Energy Procedia* **10** 106
[33] Moulin E, Paetzold U W, Bittkau K, Owen J, Kirchhoff J, Bauer A and Carius R 2013 *Prog. Photovolt: Res. Appl.* **21** 1236